GRAVITATIONAL ANOMALIES IN AND AROUND THE SALT LAKE-ALIAMANU TUFF RING COMPLEX, SOUTH-CENTRAL OAHU

A THESIS SUBMITTED TO THE UNDERGRADUATE DIVISION OF THE UNIVERSITY OF HAWAI`I AT MĀNOA IN PARTIAL FULFILLMENT
OF THE REQUIREMENTS FOR THE DEGREE OF

BACHELOR OF SCIENCE

IN

EARTH SCIENCES

December 2023

By
Benjamin Fein

Thesis Advisors
Dr. Garrett Ito
Dr. Erin Wallin

We certify that we have read this thesis and that, in our opinion, it is satisfactory in scope and quality.

THESIS ADVISORS

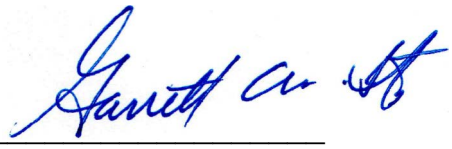

Dr. Garrett Ito, Department of Earth Sciences

Dr. Erin Wallin, Hawai`i Institute of Geophysics and Planetology

Acknowledgements

This work was funded by grant N00014-22-1-2403 from Office of Naval Research to University of Hawaii proposal number: GRANT13567133, Hydrogeology Investigations in the Moanalua and Pearl Harbor Hydrologic Units of the Honolulu Aquifer Relevant to Potential Impacts of Red Hill Bulk Fuel Storage Facility. Any opinions or interpretations are those of the author, and do not necessarily reflect the views of the University of Hawai`i or the Office of Naval Research.

I would like to thank Dr. Garrett Ito for providing me the opportunity to conduct real research and gain invaluable academic and scientific experience. Before I took on this project, I had come to Dr. Ito as a student who was unsure of what final elective course available would fill in the gaps in my knowledge that I was seeking. I was offered an opportunity to do work on a topic of both great interest and importance to the state, and I am very grateful for the experience.

I would also like to thank Dr. Erin Wallin for guiding me through the process of collecting and analyzing the gravitational data in this project, as well as providing me with valuable experience in the field to further my skills as a scientist.

Both of these people provided me with a degree of mentorship and patience that has helped me to grow tremendously over these past 12 months spent working on this project, and I am incredibly thankful for the experience of working on this report guided by them. To have the guidance of two people so willing to accommodate my unfamiliarity with this process has been invaluable in my completion of this project.

I would also like to thank my family and friends for accommodating the intricacies and oddities of my life as I worked on this project. Their love and support has been essential to me over the course of this project, and I would not have been able to complete this without them.

Abstract:

This report centers on a gravitational survey of the Salt Lake neighborhood and surrounding areas of Oahu, within a total area of roughly 6500 x 7500 meters. This survey expands on a previous survey conducted in the same area in 2019, and adds an additional 224 data points. Corrections for the effects of sample elevation (Free-Air Correction), topographic attraction (complete Bouguer correction), and the regional gravitational gradient were all removed, leaving us with a residual Bouguer anomaly. The free-air and topographic corrections were performed with a LiDAR Digital Elevation Model (DEM) which has a 1-meter spatial resolution. The regional gradient is due to the large-scale effects of the Ko'olau shield volcano, and removing its estimated effects allows us to more clearly and accurately see the local gravitational variations within our study region. The resultant residual Bouguer anomaly shows a range of approximately ±3 mGal across the range of the study area. Several distinct structures of anomalous density are evident, including a ring of low density that wraps around the northern and western sides of the Salt Lake-Aliamanu tuff ring complex, as well as a region of elevated density centered on and east of the craters. Moving northward and northeast toward the ridges and valleys of the Ko'olau shield, there is little distinguishable density variation that corresponds with topographical variations. Higher density anomalies exist to the northwest and southeast of the two craters. If the lower density areas reflect more porous subsurface materials, then this raises the possibility of these materials being more hydrologically conductive. To test this possibility, further geologic information from water well cores and further seismic and/or electrical surveys for imaging of the subsurface.

Table of Contents

List of Figures

Figure 9: Free Air Anomaly map (colors) of study area, overlying the 10-meter DEM (gray-shaded and illuminated from NW). Dots indicate measurement locations. Coordinates are UTM.

Figure 10: Simple Bouguer Anomaly map (colors) of study area, overlying the 10-meter DEM (gray-shaded and illuminated from NW). Dots indicate measurement locations. Coordinates are UTM.

Figure 11: Complete Bouguer Anomaly map (colors) of study area, overlying the 10-meter DEM (gray-shaded and illuminated from NW). Dots indicate measurement locations. Coordinates are UTM.

Figure 12: Regional Trend, consisting of a first-degree polynomial surface, with survey points shown.

Figure 13: Residual Bouguer Anomaly map (colors) of study area, overlying the 10-meter DEM (gray-shaded and illuminated from NW). Dots indicate measurement locations. Coordinates are UTM.

List of Abbreviations

Abbreviation	Definition
RHBFSF	Red Hill Bulk Fuel Storage Facility
NAVFAC	Naval Facilities Engineering Systems Command
USGS	United States Geological Survey
CBA	Complete Bouguer Anomaly
RBA	Residual Bouguer Anomaly
GNSS	Global Navigation Satellite System
DEM	Digital Elevation Model
NGA	National Geospatial Intelligence Agency
WGS	World Geodetic System
FAA	Free Air Anomaly
UTM	Universal Transverse Mercator

1. Introduction

The objective of this study is to collect and analyze gravitational survey data to map out subsurface density structures and thus give insight into the geologic structures that control groundwater flow in the Salt Lake area of Oahu. The study region lies between the Navy's fuel storage facility at Red Hill and Pearl Harbor, marked in Fig. 1 and Fig. 2. It is part of the greater Moanalua and Waimalu aquifer systems, lying directly on the border of the two watersheds. Constructed during WWII at a time when this area of Oahu was far less populated, the Red Hill Bulk Fuel Storage Facility (RHBFSF) has recently leaked fuel into the ground. This poses a serious health risk to those who draw their water from the contaminated parts of the Waimalu and Moanalua aquifers, and adds risk to contamination of a major water supply to the Honolulu area (NAVFAC, 2008). Understanding the subsurface density in the study area is an important step toward building a model of underlying rock structure and characteristics, which in turn allows for a better understanding of groundwater flow and transport around Red Hill.

Figure 1: Location map of the study area in south-central Oahu, east of Pearl Harbor in the Salt Lake neighborhood. Inset image shows the location of the study area within Oahu. (Google Earth)

Figure 2: A satellite view showing the Red Hill fuel storage facility's location within the Red Hill Ridge, with surrounding wells labeled. Distances shown are horizontal distances between wells. These wells were not used in this project. (NAVFAC, 2008)

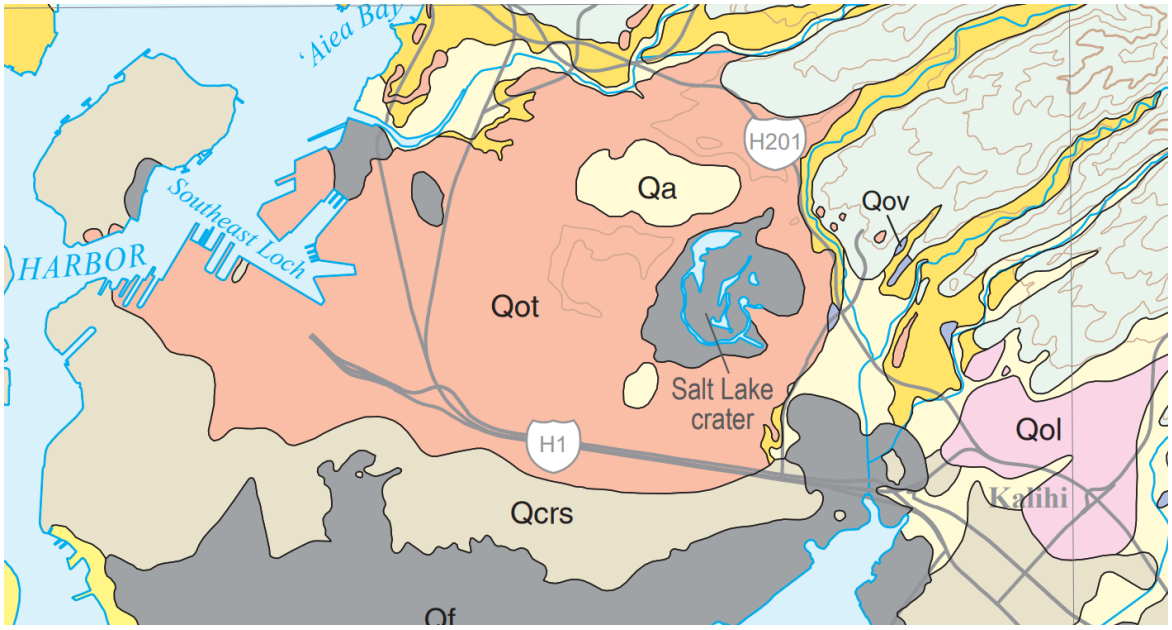

Figure 3: Geologic map of the Salt Lake-Aliamanu Tuff Rings, along with the surrounding Red Hill/Pearl Harbor area (*Study Area of Ito et al, 2019*) (USGS).

Qa - Alluvium (Holocene and Pleistocene)
Qol - Lava flows
Qov - Cinder vent deposits
Qcrs - Calcareous reef rock and marine sediment (Pleistocene)
Qf - Fill (Holocene)
Qot - Tuff Cone Deposits

The Salt Lake and Aliamanu craters are tuff rings, formed in the Honolulu Volcanics eruptive sequence during the Ko`olau volcano's rejuvenation stage. The explosivity of these eruptions is due to their phreatomagmatic nature, as these eruptions occurred just offshore of the then-coastline. The resulting combination of basaltic, tuffaceous, and carbonate deposits that compose the surface of this region today are shown in Fig. 3. This part of the Honolulu Volcanics series formed roughly 400-250,000 years ago (Ozawa et al, 2005). Rejuvenation volcanism in the Hawaiian islands is still a topic of great debate among geologists without a definitive explanation. One of the leading hypotheses suggests that the mantle experiences decompressional melting due to lithospheric flexure, well after the main shield-building stage of volcanism (Bianco et al, 2005). During hotspot volcanism, as a volcano moves over an underlying mantle plume, the huge weight of the shield volcano causes the lithosphere to flex downward beneath the growing shield volcano, and flex upward beneath the older, and more eroded volcanoes, as shown in Fig. 4. While this hypothesis is widely accepted as a part of why rejuvenation volcanism occurs, it has not been shown to fully explain the phenomenon, and more research is needed to give a more definitive explanation (Thordarson & Garcia, 2018). Regardless of their cause, rejuvenation stage volcanoes and their preceding shield stage parent volcanoes form a system of pore-rich rocks through which groundwater is able to permeate and develop aquifers, as well as denser and more impermeable dike complexes. These dike complexes are known to host groundwater, as well as structures with greatly differing hydrologic conductivities for promoting or inhibiting water flow.

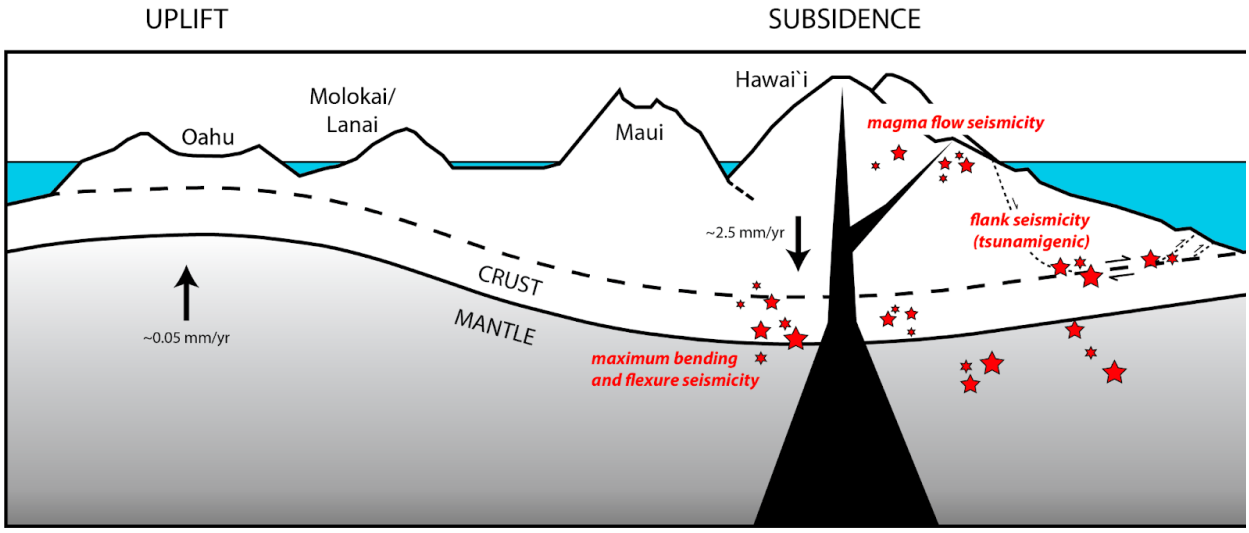

Figure 4: Cartoon of the lithospheric flexure model for rejuvenation volcanism. Decompressional melting occurs in the crust where it experiences its maximum uplift (under Oahu in this figure). (Burkhard et al, 2021).

The classic model of Oahu's groundwater and aquifer system is the Ghuyben-Herzberg lens model, which states that the groundwater is layered with freshwater at the top, transitioning to brackish water below and then saltwater at the bottom (Fig. 5). This layering has been supported by observations of freshwater discharge at submarine sites off the coast of Oahu and the Big Island, but in general is a large simplification of a complex aquifer system (Gingerich & Voss, 2005). As a relatively old Hawaiian island (the Waianae volcano erupted from 3.8-2.2 Mya), Oahu also has a developed layer of carbonate caprock along its southwestern corner. By inhibiting the seaward flow of groundwater, this maintains large freshwater aquifers near the elevation of sea level. Moving further up in elevation, Hawaiian islands also include systems of perched aquifers, caused by dike-impounded bodies of water which collect liquid from high-elevation rainfall and block the flow of water through the mountains into lower elevation aquifer systems. These features are also shown in Fig. 5. In our study area, subsurface dikes and other subsurface materials ranging from basalt to industrial and alluvial fill materials,

contribute to a variety of hydrologic characteristics and density signatures. These variations should be considered when analyzing the data collected and in interpreting the results.

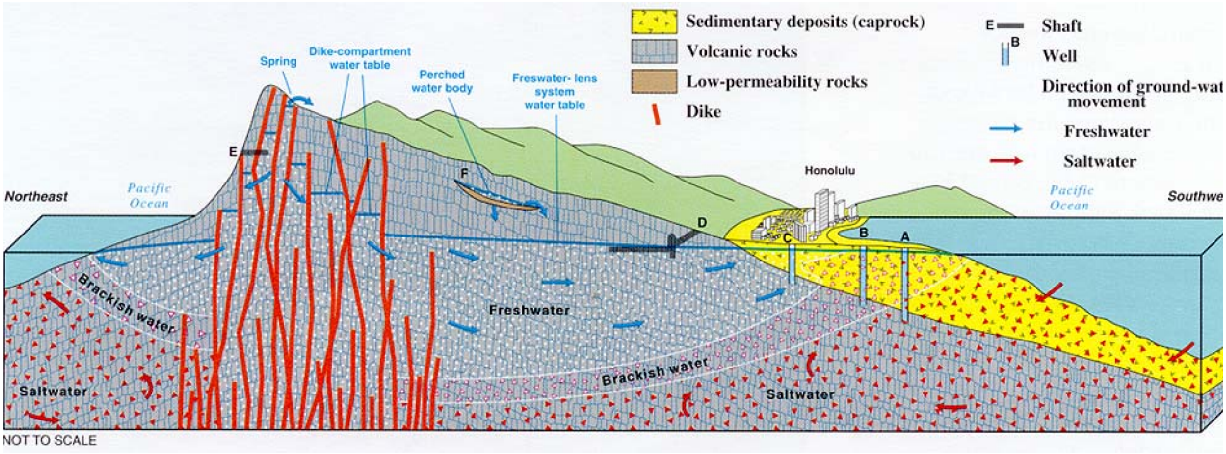

Figure 5: A schematic illustration of Oahu's aquifer system, with the Ghuyben-Herzberg water lenses, carbonate caprock, and confining dikes illustrated. The carbonate caprock prevents discharge of percolated dike-confined freshwater from rainfall into the ocean, causing pressure to build up landward of the caprocks (El-Kadi & Moncur, 2006).

The overall objective of this study is to characterize the subsurface characteristics of the study area in terms of material density. This, combined with applying prior knowledge of subsurface materials and history, will help to glean a more complete understanding of the underground materials and structures, and how they may affect the flow of groundwater in this area. In order to do this, 224 gravity measurements were collected between 11/10/2022 and 1/24/2023 and combined with 332 additional gravity measurements from Ito et al. (2019). All of the measurements were then corrected for elevation, latitude, instrument drift, tidal effects, terrain effects, and regional gravitational trends to create a series of maps, most significantly a Residual Bouguer Anomaly (RBA) which will then be analyzed for information on how the subsurface gravity anomalies could correlate to structures which may affect the flow of groundwater.

2. Methods

2.1 Gravity surveys and obtaining absolute gravity

Survey points are ideally laid out in a uniformly spaced grid, but this is often impossible in the real world. Survey points were chosen based on total areal extent, the desired spacing between measurements, and accessibility, as the study area consists largely of residential neighborhoods. A total of 224 additional data points were collected in 2022/23, and data collection continues as of the date of this report. The geographic position of each new survey point was established using a Trimble R1 GNSS Receiver. Transportation within neighborhoods was done on foot, while a pickup truck was used to transport the survey team and gravimeter between neighborhoods. The total of 536 data points from the 2019 and 2023 surveys are shown below in Fig. 6.

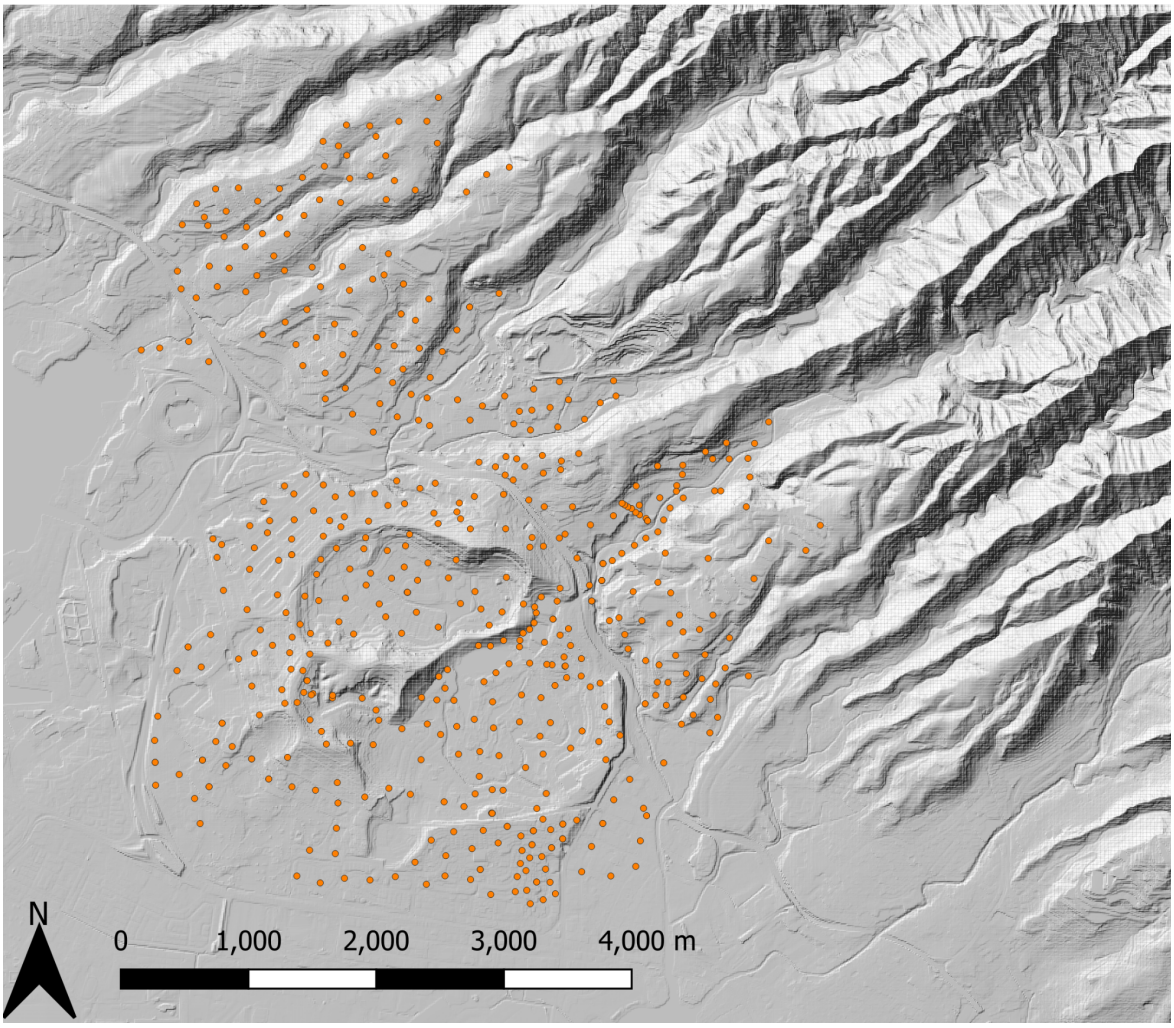

Figure 6: A Digital Elevation Model (DEM) of the Salt Lake region of south-central Oahu, with survey points marked with orange dots.

The gravimeter measures relative gravity and therefore we must convert the relative measurements to absolute gravity using a benchmark, where absolute gravity is already known. Each day of the survey began and ended by taking gravity measurements at the UH HIG Excenter benchmark. Established by the National Geospatial Intelligence Agency (NGA), this benchmark is known to have an absolute gravity value of 978944.611 ± 0.0012 mGal (Ito et al, 2019). The purpose of using a benchmark measurement is twofold, as it allows for the relative gravity readings produced by the gravimeter to be converted into absolute gravity, as well as correcting for instrument drift that occurs during the course of the day.

The drift corrections were performed using the following formula (Lillie, 1999):

$$\text{Drift Correction} = G_{Binitial} + \frac{(T_{measurement} - T_{Binitial}) \times (G_{Bfinal} - G_{Binitial})}{(T_{Bfinal} - T_{Binitial})} - G_{Bfinal} \quad (1)$$

with the following definitions:

$G_{Binitial}$ = Relative gravity reading at base station taken at start of survey

G_{Bfinal} = Relative gravity reading at base station taken at end of survey

$T_{measurement}$ = Time of field measurement being corrected

$T_{Binitial}$ = Time of gravity reading at base station taken at start of survey

T_{Bfinal} = Time of gravity reading at base station taken at end of survey

2.2 Gravity data reduction

The new data and 2018 data were combined for a total of 556 gravity measurements. In addition, thirty of the 2018 sites (selected randomly) were repeated to ensure consistency between the 2018 and 2022/23 data. After obtaining the absolute gravity at each of our measurement points, a series of reductions were done to isolate the gravitational signals due to local subsurface density structure within the crust. The first correction is to remove the major effects of the Earth's latitudinal gravity variation due to its ellipsoidal shape. Specifically, the rotation of the Earth on its axis causes it to bulge slightly at the equator. This bulge means that the distance from the center of the Earth becomes greater as one moves closer to the equator, and the force of gravity decreases accordingly. For this, we used WGS 1984 Ellipsoidal Gravity Formula used by the International Association of Geodesy (e.g., Lillie, 1999):

Eq. 1:

$$g(\phi) = 9.780325335903891718546 * \frac{1+0.001931852652458273520 87 sin^2\phi}{1-0.006694379990141316996137 sin^2\phi} mGal, \quad (2)$$

Here, ϕ is the latitude of observation point, $g(\phi)$ is the theoretical gravity for a given latitude, and g_e is the theoretical gravity at the equator (978031.85 mGal).

The next operation performed is the Free Air correction. Near the surface, gravity on Earth varies approximately linearly with elevation due to small changes in distance from the Earth's center of mass. The reduction in gravity with height *h* is roughly 0.3086 mGal for each meter gained in elevation, represented in the equation below (Lillie, 1999):

$$\Delta G_{FAA} = 0.3086\, h\,. \quad (3)$$

In this study, *h* is determined using a 1-meter LiDAR Digital Elevation Model (DEM), except for certain points in the northeastern portion of the study area that were outside the boundaries of the available 1-meter DEM files. For these data points, elevations from the Trimble GPS unit were substituted. This choice was made by comparing the GPS elevations and a 10-meter DEM against the values from the 1-meter DEM for which coverage of the study area was incomplete, it was determined that the GPS data were more accurate to the local topography than the available 10-meter DEM, and thus it was chosen as the secondary source of elevation data. We then added the correction in Eq. (3) to each measurement in an Excel spreadsheet using the equation above.

A Bouguer Slab correction is performed in order to remove the effects of mass below the topography and above sea level. The Bouguer Slab correction assumes a slab of mass extending

infinitely outward underneath each data point, with a uniform thickness and density, as illustrated in Fig. 7. The most appropriate density to use depends on the subsurface geology, which is not well known. Alluvial fill materials have different properties than vesicular basalts, for example. Oasis Montaj is a software which is able to loop through a range of density values for a Bouguer correction and find which one produces the least correlation between simple Bouguer anomaly and local topography. This did not result in any significant changes when tested between 2.60 g/cm^3 and 2.70 g/cm^3, and so I chose to stick with the standard of 2.67 g/cm^3 for the sake of parity with previous data collected and analyzed in this area by Ito et al (2019).

The Bouguer Slab correction is calculated with the following equation:

$$\Delta g = -0.04192\,\rho h \tag{4}$$

Where h is elevation in meters and ρ is rock density in g/cm^3. Using 2.67 g/cm^3 for the rock density, we are left with the following equation:

$$\Delta g = -0.1119 * h \tag{5}$$

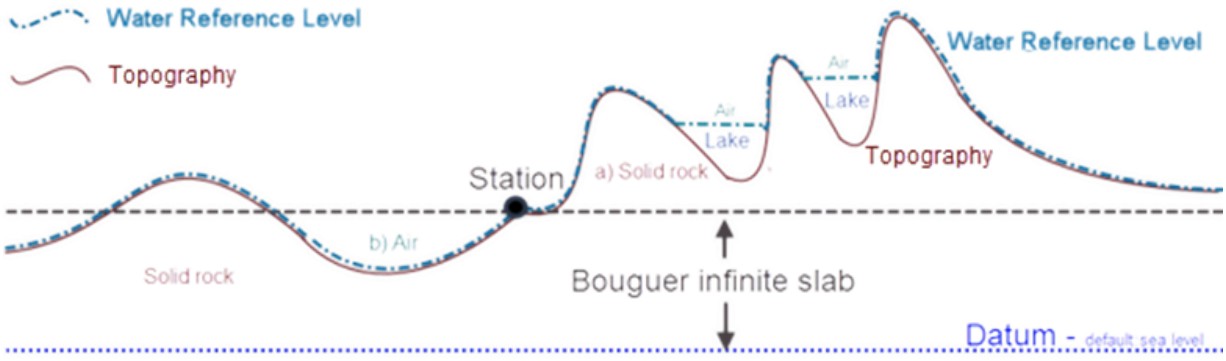

Figure 7: A 2-D schematic illustration of how a Bouguer correction is applied at a singular reference point (Seequent, 2023).

The Simple Bouguer Anomaly is produced by applying the Bouguer and Free Air corrections to the theoretical gravity value (Lillie, 1999):

$$\Delta g_B = (g - g_t) + 0.3086h - 0.04192\,\rho h \quad (6)$$

Where

Δg_B = Simple Bouguer Gravity Anomaly (mGal)

g = Measured gravity value (mGal)

g_t = Theoretical gravity value (mGal)

h = Elevation (meters)

ρ = Rock density (g/cm^3)

The final correction to be performed is the terrain correction, which removes the effect of surrounding topographic mass (mountains, valleys, etc). As performed by Oasis Montaj, this is a complex mathematical summation across 3 dimensions which relies on DEM data to model topography, as well as the density used in the Bouguer Slab correction. For each data point mapped, Oasis Montaj considers the effects of terrain radially outward, by modeling the topography as a series of rectangular prisms, each with a density 2.67 g/cm^3 and topographic height, sourced from a DEM. The lateral dimension of each prism is smallest closest to the measurement point and enlarges with increasing distance. A 2-D visual representation of how Oasis Montaj divides the correction into lower-resolution data as the radius increases is shown below in Fig. 8. Our data uses a combination of 1-meter, 10-meter, and 50-meter resolution DEMs to perform precise gravitational corrections out to distances of 50 meters, 500 meters, and 10,000 meters beyond each survey point, respectively, as opposed to the 20,000 m used by Ito et

al, (2019). The gravitational attraction of the topography was computed by summing the contributions of all grids within 10 km of each measurement point. This summed signal was then subtracted from each free air gravity anomaly point. The resulting gravity anomaly is known as the Complete Bouguer Anomaly.

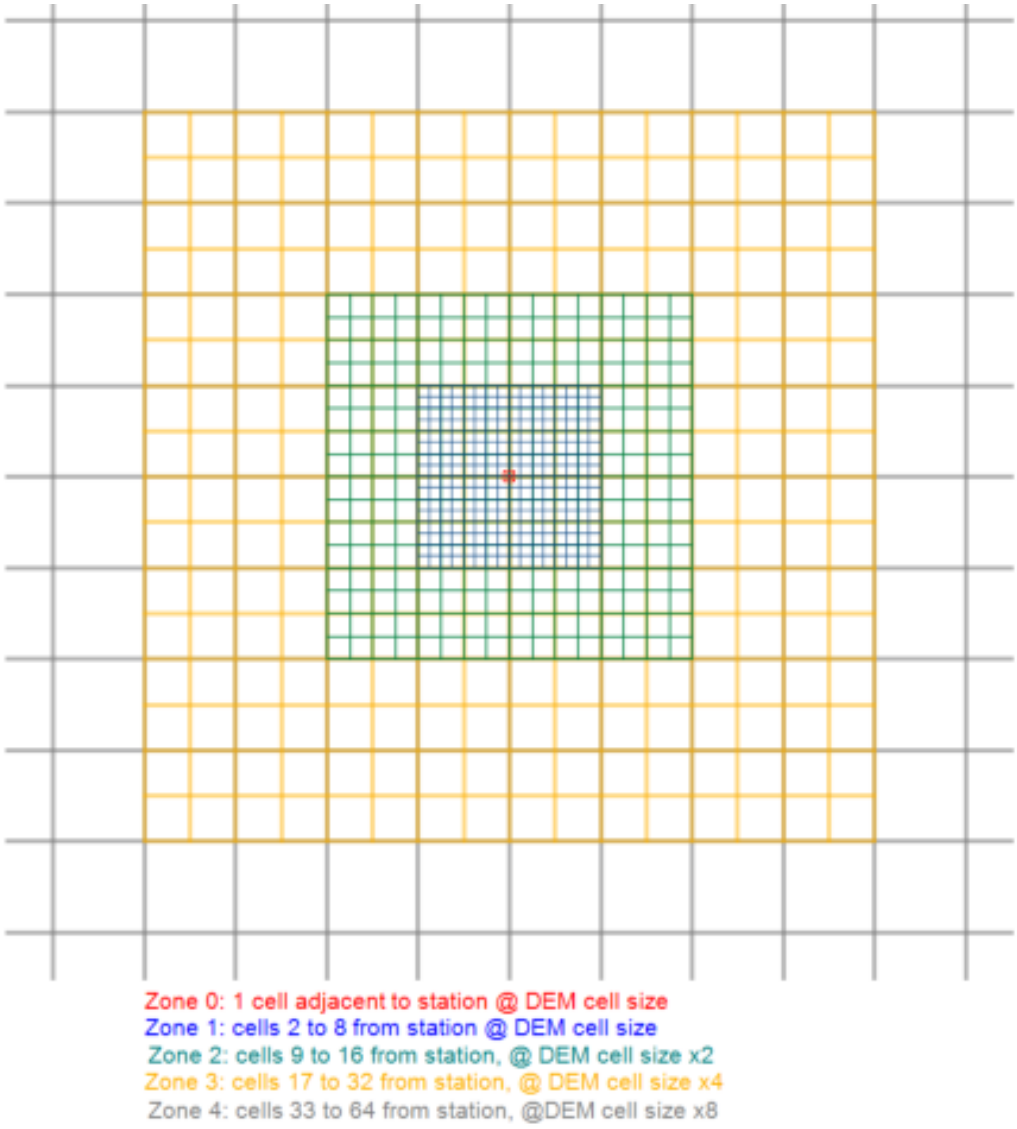

Figure 8: Simple illustration of a terrain correction performed by Oasis Montaj, dividing the surrounding topography into DEM cells of decreasing resolution corresponding to increasing radial distance (Seequent, 2023).

.

3. Results

3.1 Maps

A Free Air Anomaly (FAA) map (Fig. 9) shows the residual effects of gravity when correcting for the elevation of each measurement point above the geoid using Eq. 3 and subtracting the theoretical gravity of the ellipsoid for each point, calculated using Eq. 1. FAA maps generally show a strong correlation to existing topography, as the gravitational attraction of the topographic features in the area are responsible for the majority of signals produced. In general, gravitational highs will correspond to topographic highs, with gravitational lows corresponding to topographic lows.

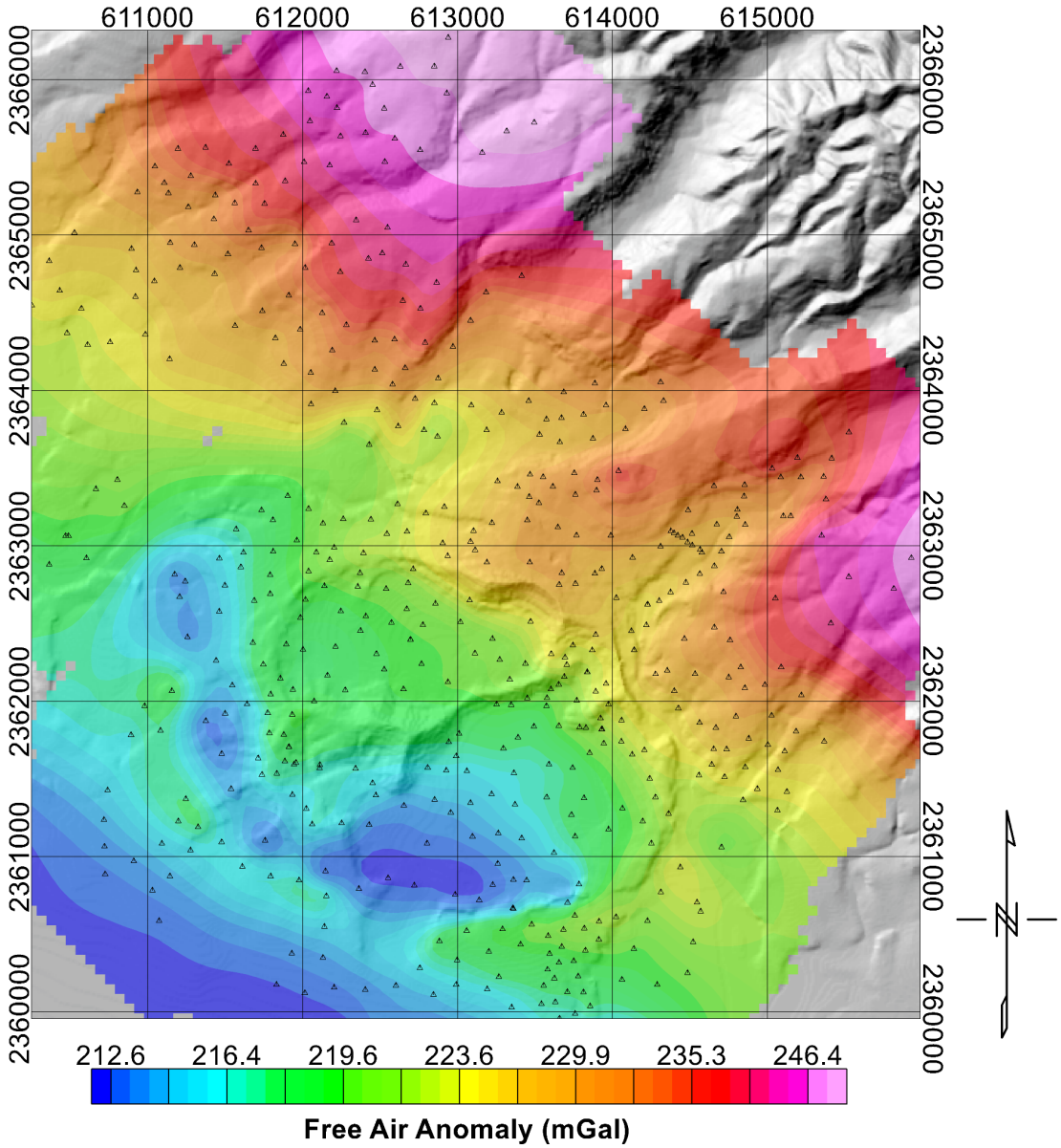

Figure 9: Free Air Anomaly map (colors) of study area, overlying the 10-meter DEM (gray-shaded and illuminated from NW). Dots indicate measurement locations. Coordinates are UTM.

A Simple Bouguer Anomaly (Fig. 10) is the resulting signal following the removal of the mass between the observation point and sea level. This anomaly therefore displays a much lower correlation with topography than the free-air anomaly, and gives a clearer view of broad-scale mass distributions in the subsurface.

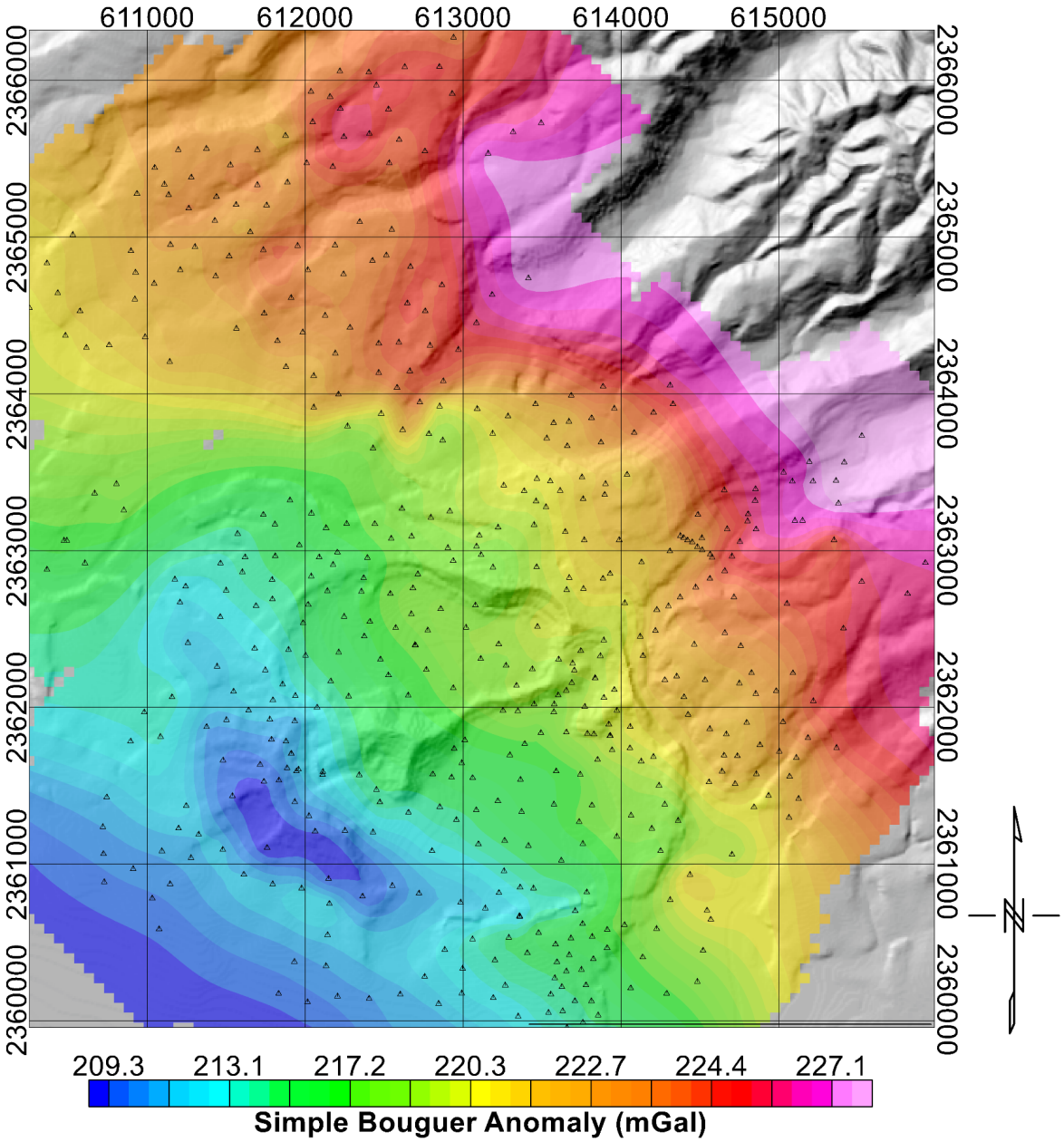

Figure 10: Simple Bouguer Anomaly map (colors) of study area, overlying the 10-meter DEM (gray-shaded and illuminated from NW). Dots indicate measurement locations. Coordinates are UTM.

A Complete Bouguer Anomaly (Fig. 11) is produced by performing a more precise terrain correction, utilizing DEMs. The resultant gravitational anomaly is now almost completely unaffected by the previously mentioned factors, and gives a more precise view of subsurface mass distribution, especially in the central and northwestern regions of the map. In

this figure, as well as the previous one, we begin to definitively see a low-gravity feature appearing to the southwest of the craters. However, as can be seen, the main features and characteristics – namely a general trend of increasing gravity to the northeast, as well as an area of anomalously low gravity in the southwest – remain very similar between the Free Air and Simple Bouguer Anomalies.

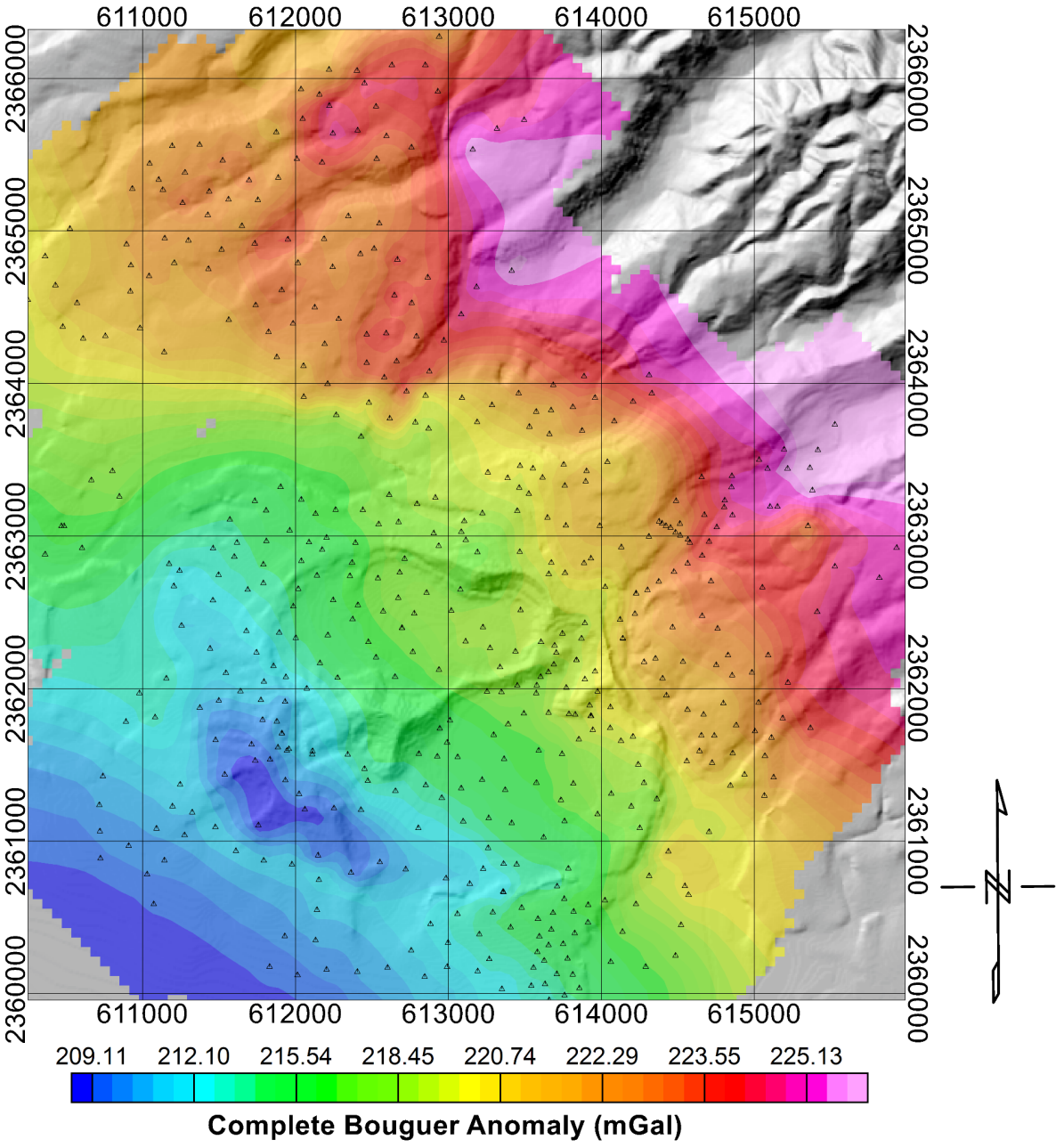

Figure 11: Complete Bouguer Anomaly map (colors) of study area, overlying the 10-meter DEM (gray-shaded and illuminated from NW). Dots indicate measurement locations. Coordinates are UTM.

The final correction performed on the data is to isolate the signal from local subsurface structure by removing a regional trend from the Complete Bouguer Anomaly. In this case, the regional trend displays an increase in gravity toward the northeast, and is associated with the mass of the Ko'olau volcano and its underlying caldera (Flinders 2013) . This trend is calculated as a best-fit polynomial surface – in this case a first-degree polynomial and shown in Fig. 12.

Regional Trend First-Degree Polynomial Surface

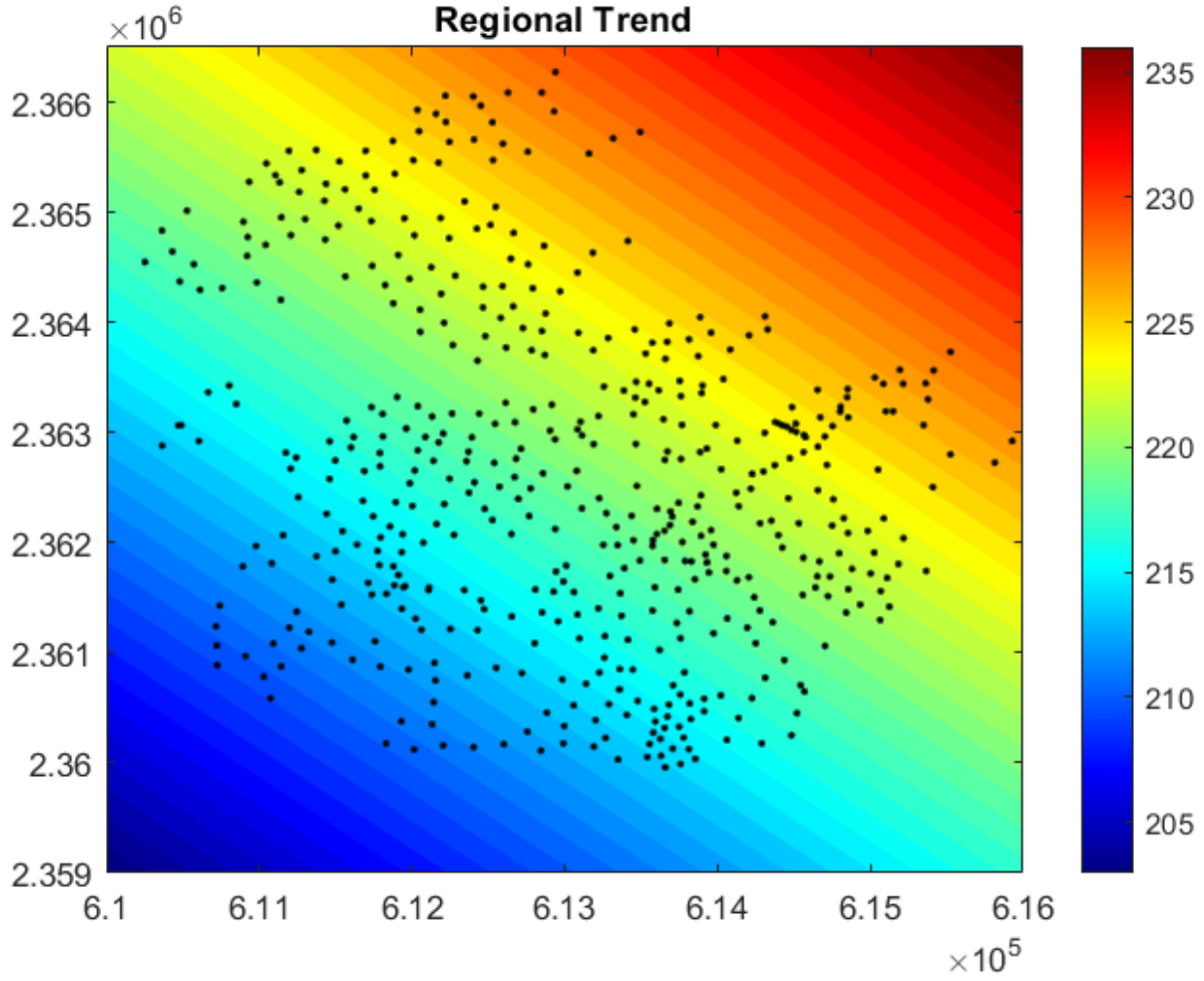

Figure 12: Regional Trend, consisting of a first-degree polynomial surface, with survey points shown.

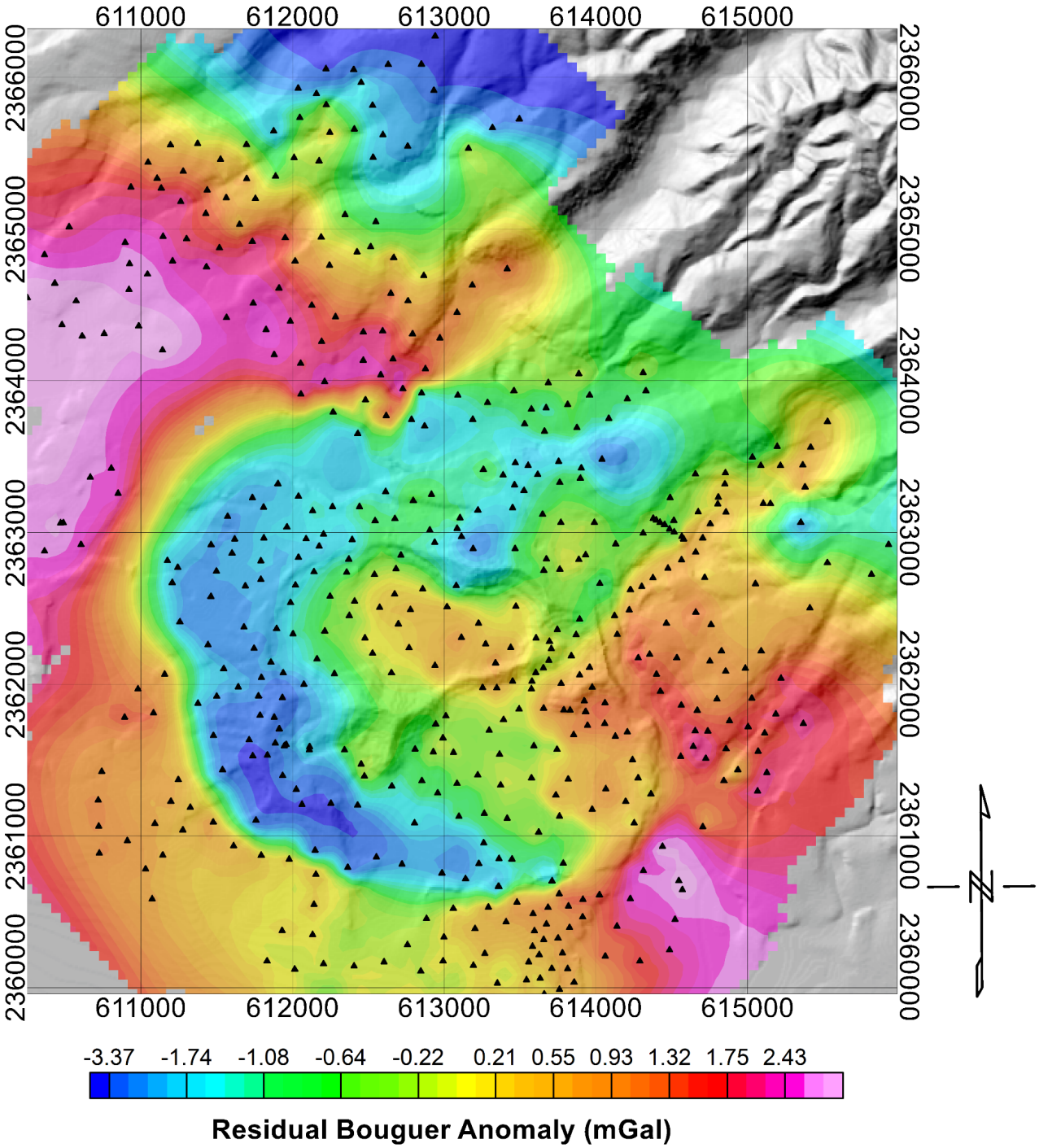

Figure 13: Residual Bouguer Anomaly map (colors) of study area, overlying the 10-meter DEM (gray-shaded and illuminated from NW). Dots indicate measurement locations. Coordinates are UTM.

Removing this planar gravity trend from the Complete Bouguer Anomaly leaves the Residual Bouguer Anomaly, in Fig. 13. This anomaly reflects the local subsurface density

structure, and in turn can give clues as to what specific types of structures may exist in the subsurface, and how they might affect groundwater flow from the aquifers to the northeast. In Fig. 13, the highest gravity is located in two regions, one to the northwest of the craters and the other to the southeast of the two craters. The lowest gravity region occurs in a singular feature which wraps around the crater complex on its south, west, and north sides. Meanwhile, features of moderately high gravity are centered on the two craters, as well as occurring to the east of the craters.

4. Discussion/Interpretations

4.1 Interpretations

The purpose of this survey is not only for use in a larger groundwater flow model, but also to help refine our understanding of the underlying structures and materials in Hawaiian rejuvenation-stage eruptions. These eruptions are not conventional shield- building eruptions which form the majority of land in the Hawaiian islands, and are largely phreatomagmatic, which contributes to their explosive nature.

Within the Honolulu Volcanics eruption series, several tuff cones are known to have erupted with phreatomagmatic mechanisms. These include Diamond Head, Punchbowl Crater, Hanauma Bay, and Koko Crater. In each of these cases, eruptions occurred underwater during a period of elevated sea levels, where layers of carbonate from reefs and other calcareous organisms had formed a layer of limestone/carbonate caprock. This layer of carbonate was subsequently punctured by these tuff cone-forming eruptions, forming an area composed of carbonate rock, existing fragmented reef materials, volcanic ash, and lithospheric xenoliths. At least one of the Salt Lake-Aliamanu crater complex eruptions occurred during a time of lower

sea levels than the present, and its eruptive products are more air-laden compared to a standard phreatomagmatic eruption (Pankiwsky, 1972). Further weathering of the Ko'olau mountains have introduced clays and other alluvial sediments to this area. The findings of this survey will help to more precisely understand the distribution of these materials underground in this area.

Current geological maps show the majority of the survey area consisting of tuff cone deposits, with areas of calcareous sediment closer to the coast, with holocene fill materials being mapped in various places as well. These maps show only the uppermost layers of material, whereas what lies below the surface is only crudely known by extrapolation (Fig. 3). Meanwhile, our current understanding of the subsurface geology of these phreatomagmatic tuff cones consists of fractured/ fragmented carbonate caprock that has been largely filled in with tuff and ash from the eruptions. Underlying this carbonate/tuff layer is generally fractured, water-bearing basalt. This gravitational survey senses density structure below the surface to depths comparable to the horizontal wavelengths (hundreds of meters to 1-2 kilometers) of the observed variations, and is able to detect the variance in these subsurface structures.

Table 1. List of relevant geologic materials and various of estimates of the associated properties (from Ito et al., 2019)

Material	Density Range (kg/m^3)	Porosity (volume fraction)	Source
Saprolite	Average: 1100 Range: 840‑1540 (dry)	Average: 0.60 Range: 0.48‑0.71	Miller, 1988; page 22
Saprolite		Average: 0.51 Range: 0.50‑0.51	Finstick, 1999
Tuff		Average: 0.44 Range: 0.22‑0.56	Finstick, 1999

Welded Tuffs	2180 +/- 230	0.141 +/-0.089	Keller, 1960
Basalt		Average: 0.43 Range: 0.05-0.51 Massive basalt: Range: 0.08-0.10 Interconnected: Range: 0.05-0.10	Nichols et al., 1996
Basalt	Average – 2400 Range: 1600-2900		Brandes et al., 2011
Basalt	2800		Visher and Mink, 1964; page 95
Basalt	1360 to 2650		Miller, 1987; page 22
Olivine Basalt	2000 to 2600		Manghanani & Woolard, 1965; page 292
Amphibolite dike	3000		Manghanani & Woolard, 1965; page 292
Olivine cumulates	3300		Flinders et al. (2013)

The most significant feature evident in the Residual Bouguer Anomaly is the inferred low-density band around the northern, southern and western edges of the volcanic craters. Table 1 lists examples of materials that are expected to be in the area along with estimates of density and porosity. Saprolite and clay are materials that have relatively low density, however, they are unlikely to be the cause of the low-density feature that rings the craters. The location of the feature, with the Salt Lake and Aliamanu craters lying between it and the Ko'olau shield, would make it unlikely that alluvial processes could fill in this area and create an anomalous low-density area. Therefore, a more likely source for the low-gravity-ring is either fractured basalts and carbonates containing air and/or fluid spaces, or eruptive tuff filling space previously

occupied by carbonate caprock, as the existing caprock in the area would have been destroyed or extensively fractured by the series of explosive eruptions. This ring of low gravity connects with a similarly low-gravity feature located at the base of Red Hill, and as such, is most likely underlain by similar materials, which may also be similar in hydrologic properties such as permeability and porosity. These results raise a new and important question: Does the low-density material provide a more permeable pathway or less permeable barrier between the base of Red Hill and around the west and south side of Salt Lake and Aliamanu craters? The answer to this question could be important to understanding the local hydrology and how fuel contaminants may move in the area. Further study should include information from water wells as well as electro-magnetic and/or seismic geophysical surveying.

Figure 5, from El-Kadi & Moncur (2006), illustrates our current understanding of the standard subsurface structures that exist in this area, interplay between tuffaceous deposits, existing and altered/ fragmented caprock, and the underlying basaltic shield. This relationship is the main factor in determining the intricacies of how groundwater behaves as it flows from the mountains towards the ocean, and the interpretations put forth in this paper are based on the assumption that this hydrogeologic model of rejuvenation-stage Hawaiian islands is accurate on a broad scale.

5. Conclusion

This study expands on a previous gravity survey conducted in 2019, and adds an additional 224 data points to the previously completed work. The steps undertaken to convert

and reduce the survey data into a Residual Bouguer Anomaly mirror those of the 2019 survey. In accordance with the previous work completed on this project, much of the resulting data from the 2019 study has not changed significantly. The most significant changes between the 2019 and 2022/23 surveys occur on the edges of the 2019 survey area, where the inclusion of further data points reveals the newly observed pattern in the Residual Bouguer anomaly. The expanded area of surveying in the far northern and western are particularly important in establishing the structure away from the craters and near the ridges overlying the Waimalu and Moanalua aquifers.

The main features uncovered by this survey are a ring of low gravity, and hence density, around the north, west, and south of the Salt Lake-Aliamanu tuff ring complex, as well as an area of higher density which occurs in the center of the craters, as well as to the east. The low-density feature is significant in that it raises the possibility of it being a more porous material which could be a hydrologic pathway for groundwater. This is of concern due to the contaminated groundwater originating from the Red Hill bulk fuel storage facility to the north of these craters. If this ring of low gravity does indeed correspond to a hydrologically porous material, then this would likely form a pathway for contaminated groundwater to flow into Pearl Harbor, as well as affecting water quality in surrounding wells and standpipes. The high-density features uncovered in this survey, meanwhile, would likely act as barriers to groundwater flow. Seeing as these features are concentrated to the center and east of the study area, they may serve to confine the contaminated groundwater to the west of these features.

Future work on this Red Hill Study Area should include examining the subsurface material recovered in rock cores, additional gravity, seismic, electrical, and electromagnetic geophysical data sets, and the continued modeling and analysis of these data. The data in this

survey, as well as future and concurrent surveys, can then be used to ultimately construct a detailed and comprehensive groundwater flow model for this region of Oahu.

References

Brandes, H.G., Robertson, I.N., and Johnson, G.P. 2011. Soil and Rock Properties in a Young Volcano Deposit on the Island of Hawaii. Journal of Geotechnical and Geoenvironmental Engineering. 137(6). 597‑610

Burkhard, L.M.L, Ward, L.A., Janiszewski, H.A., Smith-Konter, B.R., Weiss, J.R., 2021, Hawai‘i offshore quake related to tectonic plate bending, Temblor, http://doi.org/10.32858/temblor.215

El-Kadi, A.I., & Moncur, J.E. (2006). The History of Groundwater Management and Research in Hawaii.

Finstik, S.A. 1998. Subsurface Geology and Hydrogeology of Downtown Honolulu, Hawaii, With Engineering and Environmental Implications – Water Resources Project Report – PR‑99‑05. https://scholarspace.manoa.hawaii.edu/handle/10125/1989

Flinders, A.F., Ito, G., Garcia, M.O., Sinton, J.M., Kauahikaua, J., and Taylor, B. 2013. Intrusive dike complexes, cumulate cores, and the extrusive growth of Hawaiian Volcanoes. Geophysical Research Letter. 40. 3367‑3373

Gingerich, S. B., & Voss, C. I. (2005). Three-dimensional variable-density flow simulation of a coastal aquifer in southern Oahu, Hawaii, USA. *Hydrogeology Journal*, *13*(2), 436–450. https://doi.org/10.1007/s10040-004-0371-z

Gravity and terrain correction extension. Seequent. (2021, October 18). Retrieved April 21, 2023, from https://www.seequent.com/products-solutions/geosoft-oasis-montaj/gravity-and-terrain-correction-extension/

Ito, G., Higa, J., Whittier, R., Grobbe, N., Lautze, N., & Thomas, D. (2019). (rep.). *Constraints on Subsurface Density from Gravity Surveying In and Around the Salt Lake Tuff Ring Complex, South‑Central Oahu* (pp. 1–13). Honolulu, HI: SOEST.

Keller, G.V., 1960, Physical properties of tuffs of the Oak Spring Formation, Nevada: U.S. Geological Survey Professional Paper 400‑B, p. 396‑400.

Lillie, R. J. (1999). *Whole earth geophysics: An introductory textbook for geologists and geophysicists*. Prentice-Hall.

Lucas, K. (2016, April 8). *Flint-ing with disaster, the Red Hill Fuel Tanks Part 1.3*. Hawai‘i Is My MainLand. Retrieved April 3, 2023, from https://kauilucas.com/2016/04/07/flint-ing-with-disaster-the-red-hill-fuel-tanks-part-1-3/

Manghnani MH, Woollard GP. 1965. Ultrasonic velocities and related elastic properties of Hawaiian basaltic rocks. Pac Sci 19(3): 291‑295.

Miller, M.E., 1987, Hydrogeologic characteristics of central Oahu subsoil and saprolite: Implications for solute transport, M.S. thesis, University of Hawaii at Manoa, 231 p.

NAVFAC, 2008, Red Hill Bulk Fuel Storage Facility Final Groundwater Protection, p.27 https://health.hawaii.gov/shwb/files/2014/08/2008-Final-Groundwater-Protection-Plan.pdf

Nichols, W.D., Shade, P.J., and Hunt, C.D., Jr., 1996, Summary of the Oahu, Hawaii, regional aquifer‑system analysis: U.S. Geological Survey Professional Paper 1412‑A, 61 p. https://pubs.er.usgs.gov/publication/pp1412A.

NOAA Office for Coastal Management. (2023). *2013 NOAA LIDAR DEM: Oahu, HI*. 2013 NOAA Lidar DEM: Oahu, HI files. https://chs.coast.noaa.gov/htdata/raster2/elevation/NOAA_Oahu_DEM_2013_8497/

Ozawa, A., Tagami, T., & Garcia, M. O. (2005). Unspiked K–Ar dating of the Honolulu rejuvenated and Koʻolau Shield volcanism on Oʻahu, Hawaiʻi. *Earth and Planetary Science Letters*, *232*(1-2), 1–11. https://doi.org/10.1016/j.epsl.2005.01.021

Pankiwskyj, K. A. (1972). Geology of the Salt Lake Area, Oahu, Hawaii. *Pacific Science*, *26*(2), 242–253.

Thordarson, T., & Garcia, M. O. (2018). Variance of the flexure model predictions with rejuvenated volcanism at Kīlauea Point, kauaʻi, hawaiʻi. *Frontiers in Earth Science*, *6*. https://doi.org/10.3389/feart.2018.00121

USGS. (n.d.). *Geologic Map of the state of Hawai'i*. Geologic Map of the State of Hawaii. https://pubs.usgs.gov/of/2007/1089/

Visher, F.N. and Mink, J.F. 1964. Ground‑Water Resources in Southern Oahu, Hawaii – U.S. Geological Survey Water‑Supply Paper 1778. https://pubs.er.usgs.gov/publication/wsp1778.